Journal of Cleaner Production 330 (2022) 129911

Contents lists available at ScienceDirect

Journal of Cleaner Production

journal homepage: www.elsevier.com/locate/jclepro

Upcycling of waste concrete in eco-friendly strain-hardening cementitious composites: Mixture design, structural performance, and life-cycle assessment

Xiuling Li [a], Xiangrong Lv [a], Xintao Zhou [b], Weina Meng [c], Yi Bao [c,*]

[a] School of Civil Engineering, Shandong Jianzhu University, Jinan, Shandong 250101, China
[b] School of Chemical Engineering, Kunming University of Science and Technology, Kunming, 650500, China
[c] Department of Civil, Environmental and Ocean Engineering, Stevens Institute of Technology, Hoboken, NJ, 07030, United States

ARTICLE INFO

Handling editor: Cecilia Maria Villas Bôas de Almeida

Keywords:
Ductility
Flexural behaviors
Life-cycle performance
Recycled concrete powder
Strain-hardening cementitious composites (SHCC)
Sustainable and resilient structures

ABSTRACT

To upcycle waste concrete through producing strain-hardening cementitious composites (SHCC) for sustainable and resilient structures, this research investigates the effect of fine recycled concrete powder on the fresh and hardened properties, optimizes the mixture design, evaluates the structural behavior, and assesses the life-cycle performance of SHCC at material and structural levels. The investigated fresh and hardened properties include the flowability, compressive strength, tensile strength, and ductility. Four full-scale beams, including a conventional reinforced concrete beam and three reinforced SHCC beams with the optimal SHCC mixture, were tested under flexural loads until failure. Life-cycle performance of SHCC was assessed regarding the cost and carbon footprint. The results showed that appropriate use of recycled concrete powder increased the ductility while retaining the adequate compressive and tensile strengths as well as flowability of SHCC. The use of the developed SHCC with recycled concrete powder increased the load capacity and crack resistance of the full-scale reinforced beams. The developed SHCC involves higher upfront cost and carbon footprint but lower life-cycle cost and carbon footprint for the investigated structural beam applications when the service life is longer than 40 years.

1. Introduction

Concrete is one of the most widely used construction and building materials for infrastructure. Sustainability and resilience of infrastructure play vital roles in the economic wealth of a country. Compared with many other materials such as steel and lumber, concrete shows many advantages such as high construction efficiency, construction flexibility, mechanical strength, durability, and fire resistance, as well as low maintenance cost. However, the production of concrete ingredients, such as cement and aggregate, involves high carbon emission and energy consumption. On the other hand, concrete is responsible for a large percentage of construction and demolishment (C&D) waste generated from construction, maintenance, and demolition activities for structures such as buildings, bridges, and roads (Wong et al., 2018; Ho et al., 2020; U.S. EPA and Construction and Demolition). According to U.S. EPA (U.S. EPA and Construction and Demolition), U.S. generated 600 million tons of C&D waste in 2018. In the generated C&D waste, concrete was the largest portion at 67.5%, followed by asphalt concrete at 17.8%. The end-of-life management of C&D waste includes landfill or recycle. Compared with landfill, recycle of concrete is promising to minimize pollution and valorize concrete waste.

Many studies were conducted on recycling waste concrete for production of new concrete (Limbachiya et al., 2000; Sagoe-Crentsil et al., 2001; Etxeberria et al., 2007; Ma et al., 2020; Le and Bui, 2020). One of the popular methods was to produce recycled concrete aggregate (RCA), which was used to replace natural aggregate (Adams et al., 2013; Tabsh and Abdelfatah, 2009; Thomas et al., 2013; Trottier et al., 2021; Yu et al., 2019a). The method was capable of simultaneously reducing consumption of natural aggregate and minimizing volume of landfilled concrete, but it was found that the use of RCA compromised the flowability (Adams et al., 2013), mechanical strengths (Tabsh and Abdelfatah, 2009), and durability of concrete (Thomas et al., 2013). The reduction of concrete properties is attributed to the rough surface and chemical composition of RCA (Adams et al., 2013; Tabsh and

* Corresponding author.
E-mail address: yi.bao@stevens.edu (Y. Bao).

https://doi.org/10.1016/j.jclepro.2021.129911
Received 16 September 2021; Received in revised form 21 November 2021; Accepted 26 November 2021
Available online 29 November 2021
0959-6526/© 2021 Elsevier Ltd. All rights reserved.

Abdelfatah, 2009; Thomas et al., 2013). In general, RCA has porous surfaces with high water adsorption and specific surface areas, thus reducing the flowability (Adams et al., 2013); RCA has interfacial transition zones that reduce the mechanical strengths (Tabsh and Abdelfatah, 2009); and RCA has alkaline due to existence of hydration products such as calcium hydroxide (Thomas et al., 2013), thus increasing the pH value of concrete and promoting alkali-silica reaction in presence of active silica. In summary, it is an important solution to improve sustainability of structural materials by recycling C&D concrete through RCA, but resilience may be compromised. Effective measures are essential to ensure that the concrete incorporating RCA achieves desired fresh and hardened properties as well as long-term durability.

An alternative solution was to produce strain-hardening cementitious composites (SHCC) using recycled concrete. SHCC is also known as engineered cementitious composites (ECC) or ultra-high-ductility concrete (UHDC) in different contexts. Compared with conventional concrete and fiber-reinforced concrete, SHCC features strain-hardening property, superior ductility, and high crack tolerance. After SHCC is cracked under tensile stresses, it is capable of bearing higher loads, controlling the crack width to tens of micrometers, and self-healing the microcracks (Zhang et al., 2014; Li et al., 2017a, 2021). In addition, SHCC has exceptional resistance to impact loads and high temperature (Li et al., 2017b, 2018, 2019), as well as multifunctionality such as self-cleaning and air-purifying (Xu et al., 2019a, 2019b, 2020). Therefore, SHCC represents a family of resilient structural materials. To improve the sustainability, different types of recycled ingredients, such as waste glass and brick, were utilized to prepare SHCC (Guo et al., 2021; He et al., 2021; Wang et al., 2019; Yu et al., 2020). For example, a type of mixed fine particles was used to replace sand, and increased the compressive and tensile strengths as well as ductility, as elaborated in references (Wang et al., 2019; Yu et al., 2020). Recently, recycled concrete was grounded into fine particles and used to replace quartz sand in SHCC, as stated in references (Li and Yang, 2017; Gao et al., 2020, 2021; Adesina and Das, 2021). For example, recycled sand with average particle sizes ranging from 154 μm to 1074 μm was used to replace finely-grounded quartz sand (Li and Yang, 2017). The use of recycled sand increased the compressive and tensile strengths (Gao et al., 2020, 2021) while reducing the drying shrinkage (Adesina and Das, 2021), but the recycled sand reduced the durability by increasing the chloride ion penetration, permeable voids, and water absorption (Adesina and Das, 2021).

Research on using recycled concrete powder (RCP) to replace cement in SHCC is still limited (Yu et al., 2019b; Wu et al., 2021; Ji et al., 2021). RCP and brick powder were mixed and used to replace cement in SHCC (Yu et al., 2019b), and the effects of the mixed powder on the hydration kinetics and mechanical properties were evaluated. The results showed that the mixed powder increased the tensile strength and fiber-matrix bond, but reduced the ductility. In reference (Wu et al., 2021), RCP was used to replace 54% cement. The use of RCP enhanced the fiber-matrix interface but reduced the tensile strength of cementitious matrix and ductility of SHCC. In reference (Ji et al., 2021), RCP was used to replace up to 60% cement. It was found that a replacement percentage no higher than 30% increased compressive and tensile strengths while retaining the ductility of SHCC. The abovementioned studies showed the feasibility of using RCP in preparing SHCC. The following limitations were identified from the previous research on using RCP in preparing SHCC: (1) The effects of mixture design parameters on tensile properties such as the ductility were unclear. For example, some scholars claimed that the use of RCP reduced the ductility (Yu et al., 2019b; Wu et al., 2021), but other scholars argued that the ductility was retained (Ji et al., 2021). Knowledge on the effect of RCP on the mechanical properties of SHCC was lacking, and the mechanical strengths of the concrete used to produce RCP were unknown in references (Yu et al., 2019b; Ji et al., 2021). (2) The performance of SHCC with RCP in structural applications was unknown. Existing studies focused on small-scale material tests. The performance of structural elements such as reinforced concrete beams was not studied. (3) The life-cycle performance of SHCC incorporating RCP was unknown. Typically, SHCC involves high upfront costs and carbon emissions, but it is unknown whether SHCC with RCP can effectively reduce the life-cycle costs and carbon emissions of structural elements.

To address the aforementioned knowledge gaps, this research has four main objectives: (1) to investigate the effects of key mixture design variables; (2) to optimize the SHCC mixtures with RCP; (3) to test the structural performance of the optimized SHCC mixture for beam applications; and (4) to evaluate the life-cycle performance of SHCC mixtures with RCP. This research has three novelties: (1) The effects of mixture design variables are investigated, and the SHCC mixture is optimized using the Taguchi method. (2) The structural performance of the optimal SHCC mixture is tested with full-scale reinforced SHCC beams. (3) The life-cycle performance of SHCC mixtures and SHCC beams incorporating RCP is assessed at material and structural levels.

To achieve the above objectives, this study investigated the fresh and mechanical properties of SHCC mixtures and reinforced concrete beams made using SHCC. The investigated mixture design variables of SHCC included the cement replacement percentage of RCP, water-to-binder ratio, sand-to-binder ratio, fiber content, and admixture content. The investigated properties included the flowability, compressive strength, and tensile properties of SHCC, as well as flexural properties of beams made using SHCC. Finally, a life-cycle assessment of the economic and environmental performance of SHCC and beams was performed. This research is expected to promote structural applications of SHCC for sustainable and resilient infrastructure.

The remainder of the paper is organized as follows: Section 2 introduces the preparation and characterization of the RCP. Section 3 presents the experimental method and test results of SHCC mixtures incorporating RCP. Section 4 presents the experimental method and flexural test results of full-scale beams made using the SHCC. Section 5 reports the life-cycle assessment of the SHCC and full-scale beams. Section 6 summarizes the findings of this research.

2. Preparation and characterization of recycled concrete powder

2.1. Preparation

In this study, RCP was fabricated using concrete with a compressive strength of 30 MPa at 28 days. The concrete was prepared using Type I Portland cement, river sand, coarse aggregate, water, and admixtures, similar to mixtures in reference (Bao and Chen, 2015). First, concrete was cleaned by spraying tap water to remove dust attached to the surface. Then, the concrete was crushed into granules. Finally, the concrete granules were grounded to fine powder, as depicted in Fig. 1.

The concrete was crushed and grounded into fine powders via multiple steps. Between adjacent steps, the particles were dried using an oven to remove adsorbed water because water could affect the production of fine powder. Fig. 2 shows the change of the particle size through the process. Two different ball grinders with different ball size gradations were used, designated as Grinder 1 and Grinder 2. Grinder 1 had a rotating rate of 50 rpm and a grinding time of 150 min. Grinder 2 had a rotating rate of 300 rpm and a grinding time of 20 min.

2.2. Characterization

The physical and chemical properties of the RCP were characterized by standard experiments, and compared with the physical and chemical properties of Type I Portland cement and Class F fly ash that are commonly used to prepare SHCC in previous research. The investigated properties include the density, the water absorption, the loss on ignition, the particle size gradation, the chemical composition, and the morphology, as elaborated in the following.

The density of the RCP was evaluated using a Le Chatelier specific

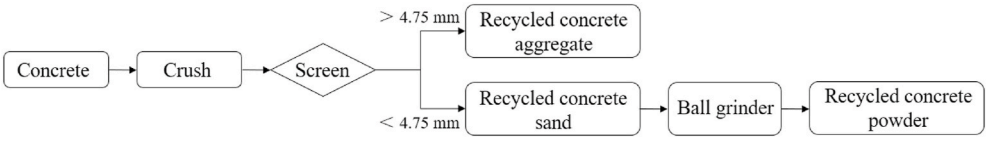

Fig. 1. Fabrication of recycled concrete powder using concrete from typical structural elements.

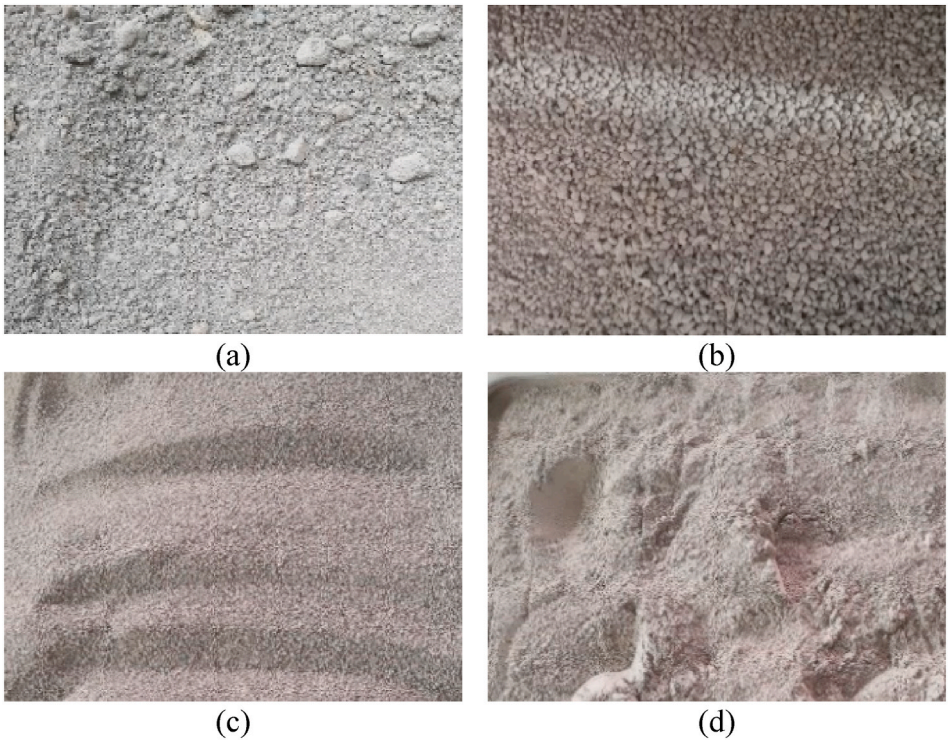

Fig. 2. Photos of concrete particles: (a) waste concrete; (b) recycled concrete aggregate; (c) recycled concrete sand; and (d) recycled concrete powder.

gravity bottle according to code (GB/T 208-2014). The specific density of the RCP was 2.632. The specific density values of Type I Portland cement and Class F fly ash were 3.126 and 2.218, respectively.

The water absorption of the RCP was evaluated according to code (GB/T 1596-2017). Sample was put in an oven with a temperature of 105 °C until the mass was stabilized. The mass loss was used to calculate the water absorption. The water absorption of the RCP was 2.1%.

The loss on ignition was evaluated according to code (GB/T 176-2017). Sample was heated to 950 °C using a high-temperature furnace until the mass of tested sample was stabilized. Then, the mass loss was measured using a high-precision balance with a precision of 1 mg, and used to calculate the loss on ignition. The loss on ignition of the RCP was 25.7%, which was higher than those of the cement (3.1%) and fly ash (2.6%).

The particle size gradation was evaluated using a particle size laser analyzer based on light scattering (Assi et al., 2018). The particle size gradation curves are plotted in Fig. 3. The mean particle size (d_{50}) values of the RCP, fly ash, and cement particles were 4.5 μm, 10.4 μm, and 12.5 μm, respectively. The results of particle size gradation indicate that the particles of the RPC are finer than the particles of the fly ash and cement.

The chemical composition was evaluated using an X-ray fluorescence (XRF) analyzer (AXS S8 TIGER) (Korf et al., 2019). The results of chemical composition are listed in Table 1. Overall, the chemical composition of the RCP is similar to that of the cement. The calcium content of the RCP is slightly lower than that of the cement but much higher than that of the fly ash.

The phase composition was determined using an X-ray diffraction (XRD) analyzer (Rigaku SmartLab) with Cu Kα radiation (1.5406 Å, 40 kV, and 20 mA) at a step size of 2°/min from 5° to 90°. Fig. 4 shows the XRD measurement results. Fig. 4(a) shows the results of the RCP, which had a large amount of calcite ($CaCO_3$) and quartz (SiO_2), as well as dolomite $CaMg(CO_3)_2$ and albite $NaAiSi_3O_8$. The calcite of fine RCP powder was expected to promote cement hydration by providing additional hydration sites and increase the mechanical strengths through

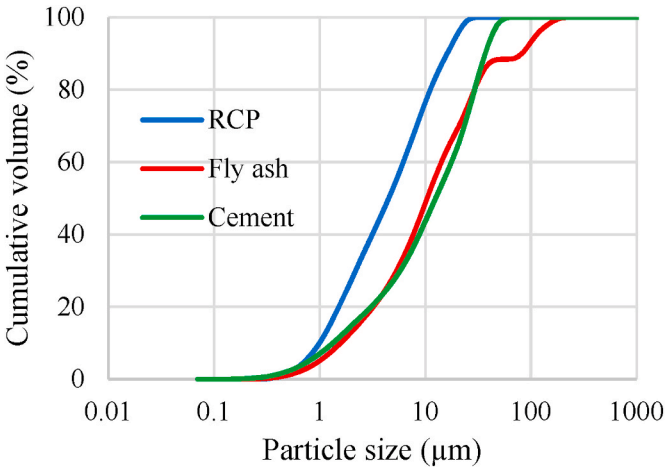

Fig. 3. Measurement results of particle size distribution of the RPC, fly ash, and cement particles.

Table 1
Chemical composition of the RCP, fly ash, and Portland cement (%).

	CaO	SiO_2	Al_2O_3	MgO	Fe_2O_3	K_2O	SO_3	Na_2O	TiO_2
RCP	44.50	23.05	6.41	2.60	2.48	1.30	0.96	0.69	0.34
Fly ash	3.32	41.00	23.39	0.93	2.97	1.34	0.96	0.48	1.21
Cement	52.09	23.64	10.48	3.42	2.33	0.76	4.26	0.37	0.57

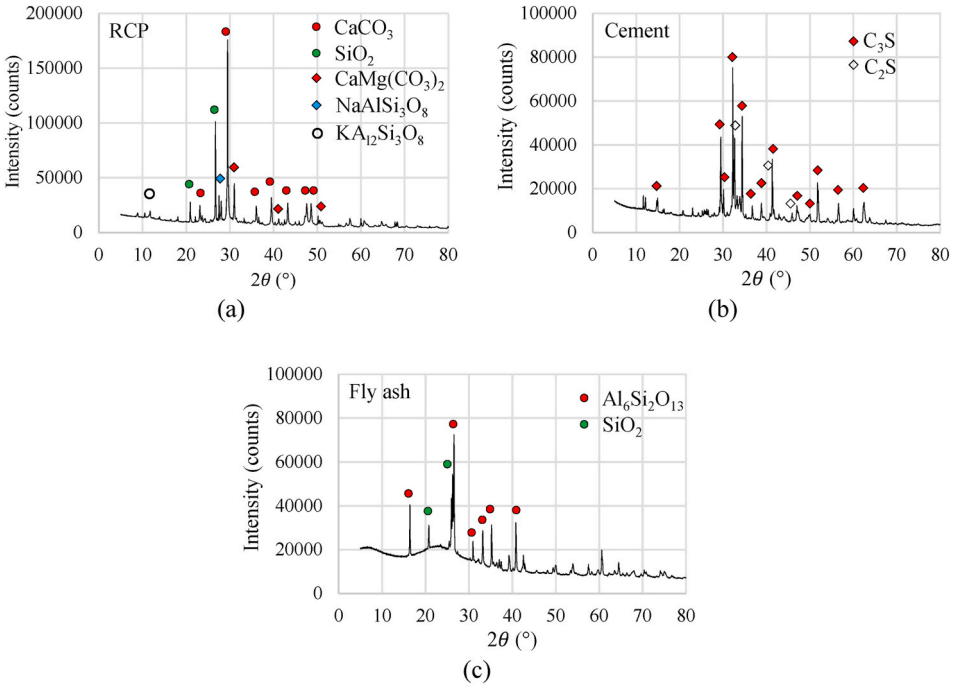

Fig. 4. Test results of XRD spectra for the different materials: (a) RCP, (b) cement, and (c) fly ash.

reaction with hydration products (Gencel et al., 2020), producing carbon aluminates and hindering production of monosulphoaluminate (AFm) (Keppert et al., 2021). It was noted that the peaks corresponding to calcium hydroxide and ettringite (AFt) were not obvious, indicating that the RCP did not have a large percentage of calcium hydroxide and ettringite. The relatively low calcium hydroxide content was attributed to the high alkalinity of the RCP proven by its high contents of K_2O and Na_2O (Table 1), which promoted carbonation of calcium hydroxide in RCP (Liu and Meng, 2021). In addition, given the large surface area of fine RCP particles, which increased the contact area between calcium hydroxide and air, carbonation occurred during the grinding process of RCP. The low ettringite content was attributed to decomposition caused by the temperature increase in the grinding process of RCP (Li et al., 2017c).

The morphology of the RCP, cement, and fly ash was respectively examined using a scanning electron microscope (SEM, model: JSM-7610F), as shown in Fig. 5. The RCP particles featured irregular shapes with acute angles, similar to cement particles, but different from spherical shapes of fly ash. The surface of RCP particles was rougher than that of cement particles because the RCP particles contained porous hydration products. It is believed that the acute angles and rough surface of the RCP particles are capable of increasing the reactivity and promote hydration reactions.

3. Mixture design and optimization

3.1. Materials

This research adopted Type I Portland cement, Class F fly ash, and RCP as binder. Finely-grounded quartz sand with a mean particle size of 75 μm was used as the fine aggregate. The specific density of the quartz sand was 2.63, and the silica content was 98.9%. Two types of chopped

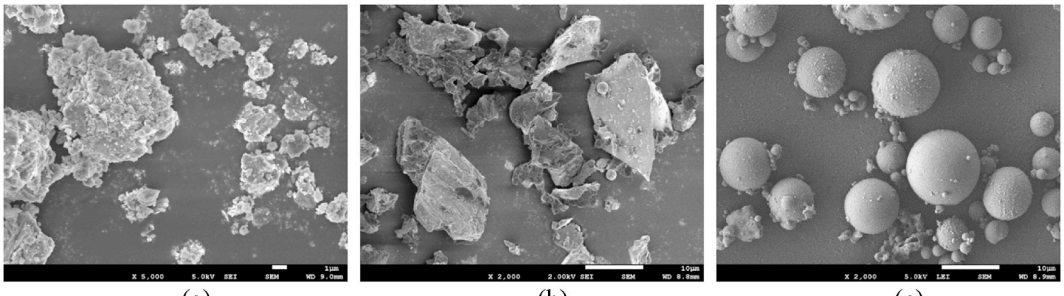

Fig. 5. SEM pictures of the particles of different materials: (a) RCP, (b) cement, and (c) fly ash.

fibers, PVA and basalt fibers, were adopted as reinforcement in SHCC. Their parameters are listed in Table 2. To improve flowability, a polycarboxylic acid-based high-range water reducer (HRWR) was used (Khayat et al., 2019).

3.2. Mixture design

Taguchi method was employed to design the tested mixtures in a L16 (4^5) table with five design variables and four levels for each variable (Liu and Tan, 2018), as listed in Table 3. The 16 mixtures were designated as M1 to M16. The five variables are the w/b at 0.24, 0.28, 0.32, and 0.36 by mass, the s/b at 0.30, 0.35, 0.40, and 0.45 by mass, the PVA fiber content at 1.0%, 1.3%, 1.5%, and 1.7% by volume, the RCP replacement percentage at 15%, 25%, 35%, and 45% by volume of RCP and cement, and the HRWR content at 0.10%, 0.15%, 0.20%, and 0.25% by mass. In the tested mixtures, Class F fly ash was used, and the fly ash content was fixed at 1.5 times the total mass of the RCP and cement. The five design variables were considered to be independent, meaning that interactions between different variables were not considered. The investigated levels of each variable are uniformly distributed in the L16(4^5) table. Each level corresponds to four mixtures, and their average results are calculated to represent the corresponding level. For instance, the average result of the mixtures M1 to M4 represents the result corresponding to the w/b at 0.24.

3.3. Test methods

The mixtures were mixed using a 19-L Hobart mortar mixer. First, the binder and quartz sand were mixed in dry condition at 60 rpm for 2 min. Then, the HRWR was dissolved in water and added into the mixer, followed by mixing at 120 rpm for 8 min. Next, the basalt fibers were added to the mixer, followed by mixing at 120 rpm for 2 min. Finally, the PVA fibers were added, followed by mixing at 120 rpm for 2 min. After the mixing, the mixture was examined by hand, and no fiber agglomeration or segregation was found.

The flowability of the mixtures was evaluated using the slump spread on a jump table according to code (GB/T 2419-2005). Each test was duplicated for three times, and the results were averaged. Then, the mixtures were used to cast the specimens for evaluating the hardened properties. All specimens were covered with wet burlap and plastic sheet immediately after casting at 22 ± 2 °C. The specimens were stored at 22 ± 2 °C for 24 h, and then, the specimens were demolded and cured in an environmental chamber at 22 ± 2 °C and a relative humidity of 95 ± 5% until the age of testing. The compressive strengths of the mixtures were evaluated at 7 days and 28 days. The tensile properties were evaluated at 28 days.

The compressive strengths were evaluated using 70.7 mm cubic specimens in accordance with standard JGJ/T70-2009 (J/T70-2009. Standard fo, 2009). The cubic specimens were tested using a load frame (load capacity: 100 kN) at a rate of 500 N/s. The tensile behaviors were tested using dog-bone specimens with a cross section of 30 mm × 13 mm, as depicted in Fig. 6(a). The specimens were tested using a load frame at a rate of 0.15 mm/min. The applied load and elongation were respectively measured using a load cell (load capacity: 10 kN) embedded in the load frame and a clip-on gauge. The measuring range of the clip-on gauge was ±12.5 mm. Fig. 6(b) plots the tensile stress-strain curves of mixtures M9 and M10 (see more curves in Appendix). The stress was calculated by the tensile force divided by the cross section (30 mm × 13 mm). The strain was calculated by the elongation divided by the gauge length. The tensile strength and ductility were defined as the peak tensile stress and ultimate strain, respectively. Each test was repeated for three times, and the results were averaged.

Table 2
Parameters of chopped fibers.

	Length (mm)	Diameter (μm)	Specific density	Tensile strength (MPa)	Ductility (%)	Elastic modulus (GPa)
PVA	12	39	1.3	1620	8	42.8
Basalt	18	15	2.65	2320	2.6	84.5

Table 3
Mixture design.

Mixture	w/b	s/b	PVA fiber content (%)	RCP replacement percentage (%)	HRWR content (%)	Basalt fiber content (%)
M1	0.24	0.30	1.0	15	0.17	0.2
M2	0.24	0.35	1.3	25	0.20	0.2
M3	0.24	0.40	1.5	35	0.23	0.2
M4	0.24	0.45	1.7	45	0.25	0.2
M5	0.28	0.30	1.3	35	0.25	0.2
M6	0.28	0.35	1.0	45	0.23	0.2
M7	0.28	0.40	1.7	15	0.20	0.2
M8	0.28	0.45	1.5	25	0.17	0.2
M9	0.32	0.30	1.5	45	0.20	0.2
M10	0.32	0.35	1.7	35	0.17	0.2
M11	0.32	0.40	1.0	25	0.25	0.2
M12	0.32	0.45	1.3	15	0.23	0.2
M13	0.36	0.30	1.7	25	0.23	0.2
M14	0.36	0.35	1.5	15	0.25	0.2
M15	0.36	0.40	1.3	45	0.17	0.2
M16	0.36	0.45	1.0	35	0.20	0.2

3.4. Test results and discussion

The test results of the fresh and mechanical properties of the mixtures are shown in Table 4. According to Taguchi method, the effect of each variable on a property of the mixture was reflected by the statistic results of different levels of the variable. Since the variables and levels of each variable were uniformly distributed in the L16(4^5) table, the result corresponding to each level of a variable was calculated as the average of the mixtures with the same level.

According to the Taguchi method, the effects of the different mixture design variables were calculated based on the L16(4^5) table. In each plot, the data point represented the average of the results from different mixtures with the same level for one variable, and the error bar represented the standard deviation of different mixtures. Fig. 7(a) shows the effects of the mixture design variables on slump spread. The flowability increased with w/b and the HRWR content, and decreased with the fiber content and RCP content, consistent with previous research (Meng et al., 2017). The fiber content had the highest effect on the flowability, followed by w/b and RCP content. The fibers had high water adsorption and interlock effects. The high water adsorption reduced free mixing water, so both the high water adsorption and interlock effects reduced the flowability. The reduction of flowability with the increase of RCP content was attributed to two main mechanisms. The rough surface of RCP increases inter-particle friction. The rough surface and small size of RCP particles increase the specific surface area and the water adsorption. The reduction of flowability tends to entrap air and increase porosity, thus reducing the flowability.

Fig. 7(b) and (c) show the effects of variables on the compressive strengths at 7 days and 28 days, respectively. The compressive strengths decreased with w/b and RCP content, and w/b had the highest influence. The increase of w/b introduced more pores in the matrix, thus reducing the compressive strengths. When the RCP content was lower than 25%, increasing the RCP content increased the compressive strengths, because the fine particles promote hydration reactions (Yu et al., 2019b). When the RCP content was higher than 25%, increasing the RCP content reduced the compressive strengths due to two effects: (1) The RCP diluted the cement content and reduced the content of hydration products. (2) The RCP reduced the flowability and entrapped more air to the matrix, causing air voids that represented defects, thus

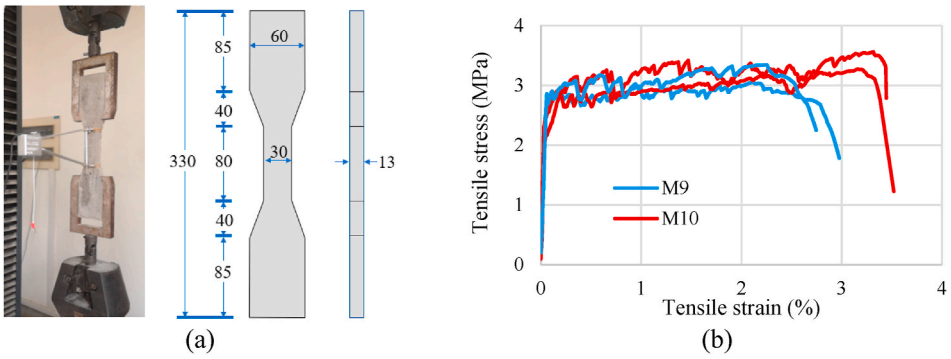

Fig. 6. Depiction of the tensile tests: (a) test setup and specimens (unit: mm); and (b) representative results of stress-strain relationships from mixtures M9 and M10.

Table 4
Test results of the investigated SHCC mixtures.

Mixture	Slump spread (mm)	7-day compressive strength (MPa)	28-day compressive strength (MPa)	28-day tensile strength (MPa)	28-day ductility (%)
M1	240	28.60	39.30	3.15	0.20
M2	180	31.50	47.30	4.20	0.80
M3	172	24.28	37.90	4.59	1.12
M4	158	17.20	31.40	4.20	1.40
M5	217	15.37	22.26	3.69	1.18
M6	215	15.97	29.40	3.17	0.86
M7	185	18.89	27.96	3.52	1.16
M8	185	23.52	34.09	4.36	0.88
M9	200	11.16	21.51	2.80	2.40
M10	187	15.40	25.70	3.61	3.32
M11	245	19.60	30.86	2.94	1.12
M12	230	17.80	25.30	2.94	0.64
M13	235	15.90	19.50	3.01	0.42
M14	240	17.55	20.16	2.65	0.32
M15	200	12.58	27.83	3.36	2.24
M16	255	13.40	25.00	2.34	0.80

reducing the compressive strength (Meng and Khayat, 2017). The effects of the other three variables were relatively small compared with the w/b and RCP content.

Fig. 7(d) shows the effects of variables on the tensile strength at 7 days. The tensile strength decreased with w/b and slightly increased with s/b, fiber content, and RCP content. The increase of w/b increased the porosity of matrix and thus reduced the tensile strength. When s/b was low, quartz sand helped tune the matrix and fiber-matrix interface and promote generation of multiple cracks in the matrix while hindering localized fracture, thus improving the tensile strength (Li, 2003). When s/b was high, the strength of the matrix was highly reduced, thus reducing the tensile strength. The increase of the fiber content enhanced the bridging effect at cracks, thus enhancing the tensile strength. The influence of RCP content on the tensile strength was the result of the two competing effects (Li, 2019): (1) The RCP particles promoted hydration reactions, thus refining the microstructures of matrix and enhancing the fiber-matrix interface bond strength. (2) The RCP particles reduced the tensile strength due to the dilute effect and flowability reduction of the mixture. When the RCP content was no higher than 25%, the promoting effect was dominant, and, therefore, the tensile strength increased with the RCP content. When the RCP content was higher than 25%, the reducing effect was dominant.

Fig. 7(e) shows the effects of the five mixture design variables on the ductility at 7 days. The ductility first increased and then decreased with the increase of w/b. When w/b was low, the increase of w/b weakened the tensile strength of the matrix and the bond strength of the fiber-matrix interface. The weakening effect promoted generation of multiple microcracks in the matrix, thus increasing the ductility. When w/b was high, the matrix was weak and controlled the failure, so further increasing w/b reduced the ductility. The ductility first increased and then decreased with the increase of s/b, following the similar trend with w/b. The increase of fiber content enhanced the fiber bridging effect at cracks, thus enhancing the ductility. The increase of RCP content improved the ductility because RCP particles modified the fiber-matrix interface bond and in turn the fiber bridging effect (Bao and Li, 2020). In addition, overall, the RCP particles tended to reduce the strength of the matrix, as reflected in Fig. 7(b) and (c), and the reduction of the matrix strength also improved the ductility when the failure was controlled by fiber rupture. It should be noted that there is a tradeoff between the mechanical strengths and the ductility when the RCP content is higher than 25%. As the RCP content increased from 25% to 45%, the mechanical strengths were reduced, but the ductility was increased. Such a tradeoff should be noted in structural applications of SHCC incorporating high-volume RCP because both the mechanical strengths and ductility play important roles in engineering structures.

According to the test results of mixtures designed using the Taguchi method, the effects of the investigated mixture design variables were ranked as: (1) w/b, (2) RCP content, (3) fiber content, (4) s/b, and (5) HRWR content. The ranking was made based on the effects of the investigated variables on the fresh and mechanical properties of the tested mixtures. It should be noted that the ranking of variables is dependent on the investigated ranges of the variables. Based on the test results, the Taguchi method was employed to determine the optimal mixture that was capable of achieving the overall best performance in terms of the fresh and mechanical properties, as shown in Table 5. The fresh and mechanical properties were tested to verify the optimal mixture. The test results are shown in Table 6.

4. Flexural testing of beams

This section presents flexural testing of four full-scale beams commonly used in buildings. Three beams were made using the optimal mixture, and one beam was made using conventional concrete. They were tested until failure to evaluate the load capacity, ductility, and crack patterns.

4.1. Specimens

The three beams made using the SHCC mixture were designated as SHCC-1 to SHCC-3. The beam made using conventional concrete was designated as CC. The conventional concrete beam was the control specimen. The mixture design of concrete is shown in Table 7. The compressive strength at 28 days was 30 MPa.

The four beam specimens were designed to exhibit flexural failure with yielding in steel bars and crushing in concrete. This study also evaluated the effects of reinforcement ratio on the flexural behaviors. The control specimen CC had a reinforcement ratio of 1%, and specimens SHCC-1 to SHCC-3 respectively had reinforcement ratios of 1%, 1.57%, and 0.26%. Fig. 8 shows the geometry and reinforcement of the

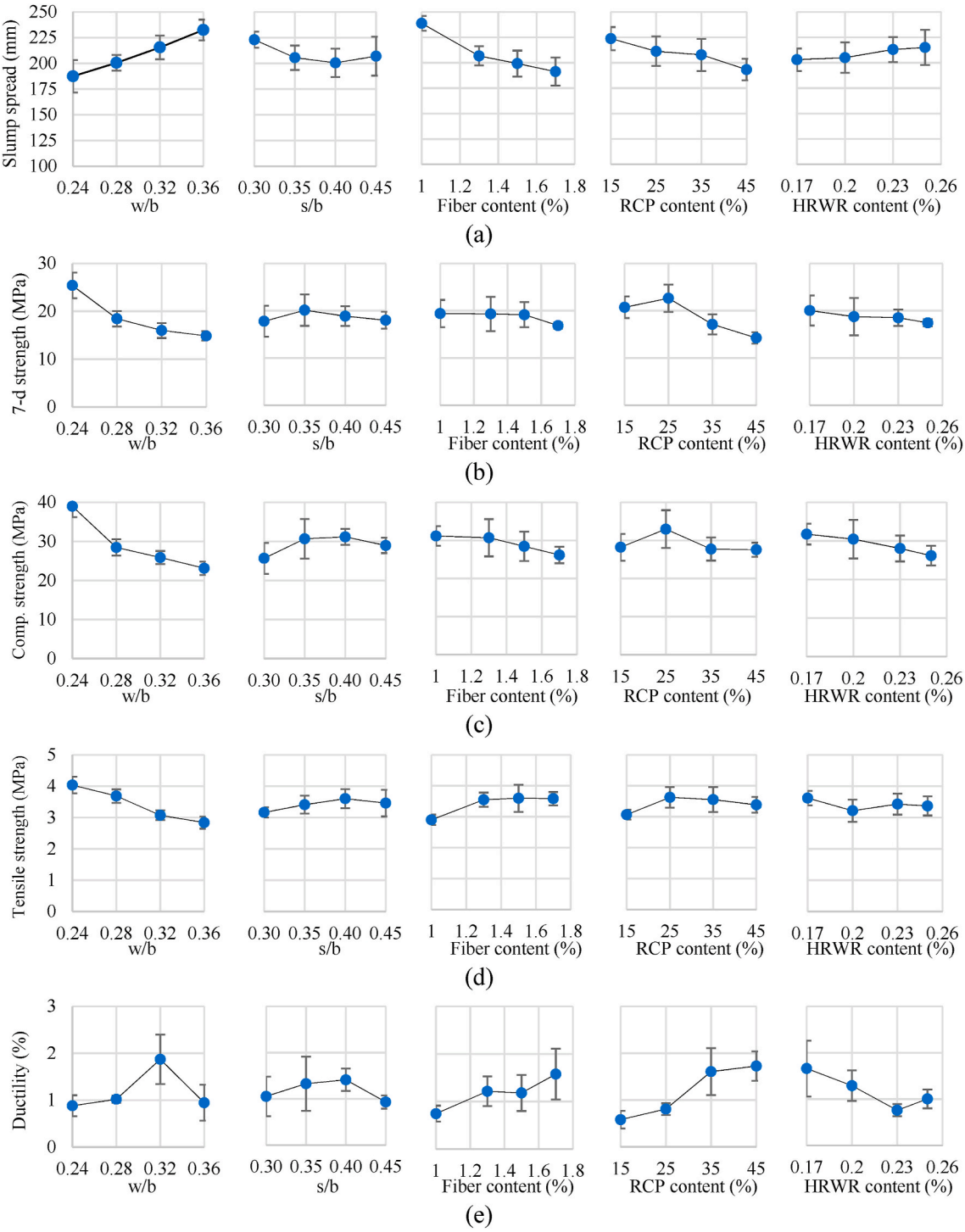

Fig. 7. Test results: (a) slump spread, (b) 7-day compressive strength, (c) 28-day compressive strength, (d) 28-day tensile strength, and (e) 28-day ductility.

Table 5
Proportion of the optimal mixture.

RCP replacement percentage (%)	w/b	s/b	PVA fiber content (%)	HRWR content (%)	Basalt fiber content (%)
45	0.32	0.40	1.7	0.17	0.2

Table 6
Fresh and mechanical properties of the optimal mixture.

Slump spread (mm)	7-day compressive strength (MPa)	28-day compressive strength (MPa)	28-day tensile strength (MPa)	28-day ductility (%)
180	13.8	30.2	3.98	1.15

Table 7
Mixture design of the conventional concrete (kg/m^3).

Portland cement	River sand	Coarse aggregate	Water	HRWR
440	700	1050	167.2	4.4

beams. Three diameters of deformed steel bars were used as the longitudinal bars: Φ8, yield strength 420 MPa; Φ10 and Φ16, yield strength 445 MPa; and Φ20, yield strength 430 MPa. The elastic modulus of the steel bars was 205 GPa.

4.2. Test setup and instrumentation

The beams were tested under a four-point bending setup, consistent with the setup in reference (Tan et al., 2021), as illustrated in Fig. 9. Each beam was supported by two rollers placed on a strong floor and loaded using a hydraulic actuator with a load capacity of 300 kN. The load was applied to the beam through a rigid spreader beam. The applied load was under displacement control, and the loading rate was 2 mm/min. The span length between the supports was 2700 mm, and the distance between the two loading points was 900 mm. A load cell was placed between the actuator and spreader beam to measure the applied force. Five linear variable differential transformers (LVDTs) were used to measure the displacement of the beam at critical sections. The five LVTDs are designated as LVDT-1 to LVDT-5. Electric resistance strain gauges were deployed on the longitudinal steel bars in the tensile zone at the middle span, as shown in Fig. 4(a).

4.3. Test results and discussion

4.3.1. Failure process and crack pattern

In specimen CC, the first crack was generated at the bottom surface near the middle span when the applied load reached 10 kN, and the crack width was 0.03 mm. As the load was increased, more cracks were generated in the flexural span, and the crack width was increased. The first crack in the shear span was generated when the applied load reached 40 kN, and the crack width was 0.05 mm. As the load was increased, more cracks were generated in both the flexural and the shear spans, accompanied by widening of cracks. After the mid-span deflection reached 40 mm, a crack near the middle span was developed and formed a major crack with a crack width wider than 2.5 mm, and led to flakes of concrete, so the LVDT at the middle span was removed to avoid damages. Finally, the beam failed with yielding in steel bars and crushing of concrete near the middle span.

In the three SHCC beams, the first crack was also generated at the bottom surface near the middle span when the applied load reached 10 kN, but the crack width was smaller than 0.01 mm. As the load was increased, more cracks were generated in the flexural span, and the crack width was less than 0.02 mm until cracks were generated in the shear spans. The first crack in the shear span appeared when the applied load was increased to 65 kN for specimen SHCC-1, 60 kN for specimen SHCC-2, and 55 kN for specimen SHCC-3. The crack width was 0.03 mm. As the load was further increased, more cracks were generated in the flexural and shear spans, accompanied by widening of existing cracks, until the specimens failed with yielding in steel bars and minor crushing of SHCC near the middle span. The formation and development of the cracks were accompanied by sound of fiber rupture, but no flaking of SHCC was observed. For specimen SHCC-1, after the mid-span deflection reached 40 mm, a major crack near the middle span was formed with a crack width of 2.3 mm. For specimen SHCC-2, after the mid-span deflection reached 20 mm, a major crack near the middle span was formed with a crack width of 2.2 mm. For specimen SHCC-3, after the mid-span deflection reached 20 mm, a major crack near the middle span

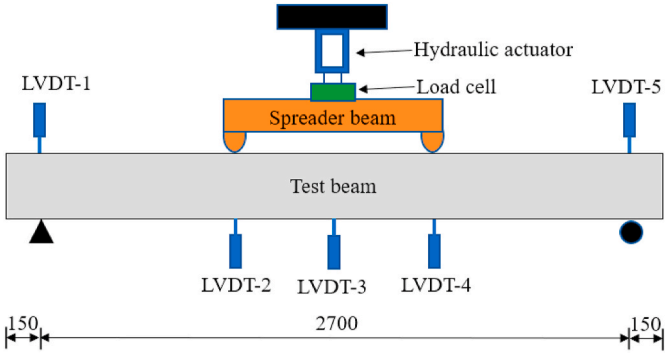

Fig. 9. Illustration of the four-point bending test setup and the instrumentation of the tested beam specimens. (Unit: mm).

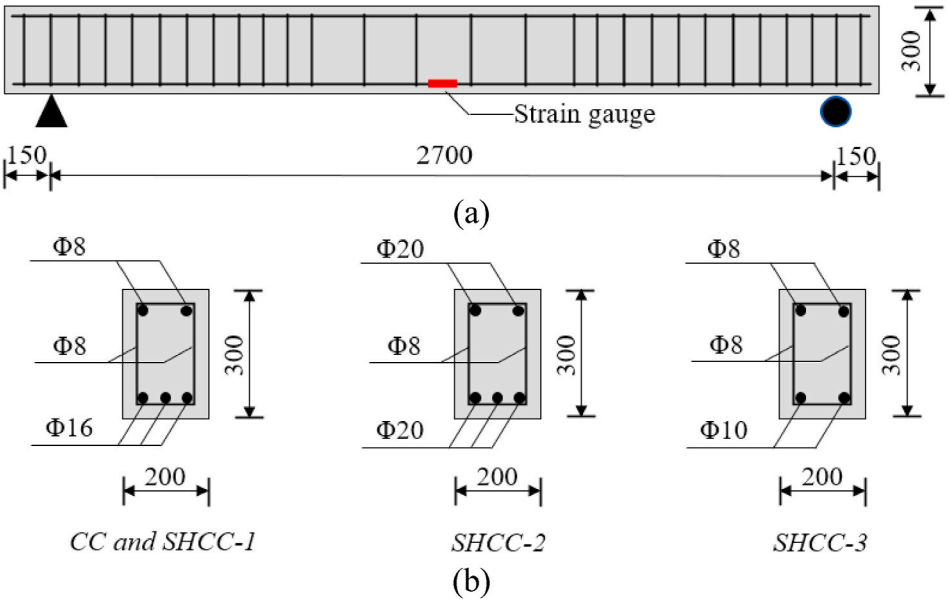

Fig. 8. Illustration of the geometry and reinforcement layout of the investigated beam specimens: (a) the elevation view, and (b) the cross sections of the different specimens. (Unit: mm).

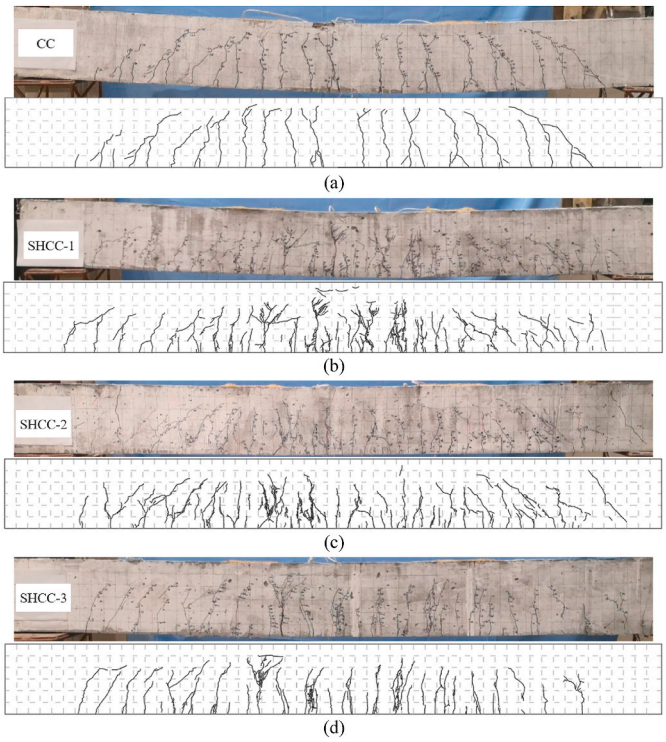

Fig. 10. Crack patterns of the specimens: (a) CC, (b) SHCC-1, (c) SHCC-2, and (d) SHCC-3.

was formed with a crack width of 2.0 mm.

The crack patterns of the four beams are plotted in Fig. 10. Compared with the control specimen, specimen SHCC-1 with the same reinforcement ratio as the control specimen exhibited more microcracks and minor crushing in the compression zone when the beam failed. The more microcracks were attributed to the intrinsic capability of crack width control of the SHCC under increasing tensile loads, and the capability of crack width control of the SHCC was due to the mechanistically-tuned microstructures, as elaborated in reference (Li, 2019). Due to the bridging effect of the fibers, the matrix of SHCC is cracked to release energy and accommodate the increasing loads, delaying widening of cracks (Li, 2019). The formation of microcracks was capable of improving the ductility and energy dissipation capacity as well as the long-term durability of the SHCC beams, because presence of microcracks has little effect on the permeability (Li, 2019). For specimens SHCC-1 to SHCC-3, the increase of the reinforcement ratio generated more cracks and reduced the width of the major crack that caused localized damage when the beams failed, but the reinforcement ratio did not show significant effects on the widths of the distributed cracks before the formation of the major crack in the SHCC beams, because the SHCC intrinsically controlled the crack widths.

4.3.2. Load-displacement curves

Fig. 11 shows the load-deflection curves of the beams. The deflection is the mid-span deflection. The results of the four beams showed the same trend. First, the load increases with the mid-span deflection approximately linearly, until many cracks are generated. With the propagation and widening of cracks, the increasing slope is reduced, until the load reaches the peak. Then, the load starts to decrease. Due to use of steel bars, the load does not drop rapidly after the load peak. The first cracking points are marked using a red circle. Specimen SHCC-1 demonstrated the higher load-carrying capacity than the control specimen because SHCC was capable of bearing higher tensile forces after it was cracked. Although specimens SHCC-1 and CC had the same steel reinforcement ratio, specimen SHCC-1 had additional reinforcement due

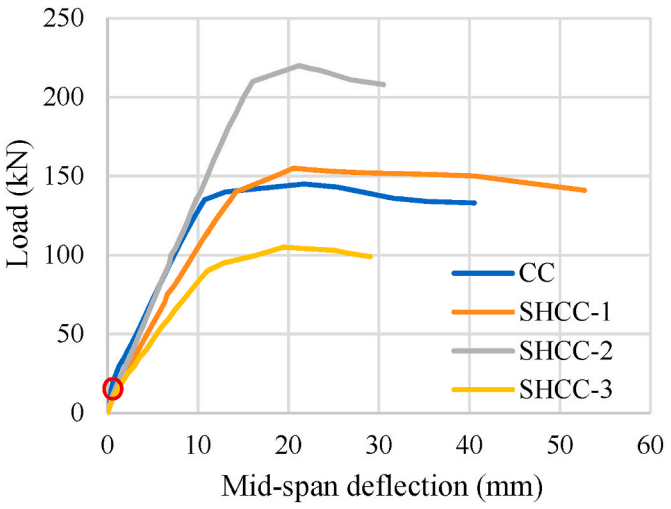

Fig. 11. Load-deflection curves of the investigated specimens tested under four-point bending.

to the use of chopped fibers. At the cracks, SHCC was able to carry a certain percentage of tensile forces, alleviating the tensile force in the steel bars. The use of SHCC increased the load-carrying capacity by 8%. The increase of the load-carrying capacity was attributed to the additional tensile resistance provided by the chopped fibers that delayed the yielding of steel bars in the SHCC beams. Meanwhile, the increase of the reinforcement ratio significantly increased the load-carrying capacity of the beams. As the reinforcement ratio was increased from 0.26% to 1.57%, the load-carrying capacity was increased by 110%, and reasonable ductility was sustained, indicating that the reinforcement ratios of the beams were appropriate with the incorporation of the SHCC mixture. The independence of the load-carrying capacity on the reinforcement ratio also explains the effect of the SHCC.

4.3.3. Strains in steel bars

Fig. 12 shows the load-strain curves of longitudinal steel bars in tension zones of the beams. Specimen SHCC-1 had lower strains than the control specimen after cracking, corroborating the analysis on the bridging effect of chopped fibers in Section 4.3.2. The use of the SHCC mixture reduced the strains in the steel bars, and thus increased the load-carrying capacity of the beam. Comparison of specimens SHCC-1 to SHCC-3 revealed that the increase of the reinforcement ratio also

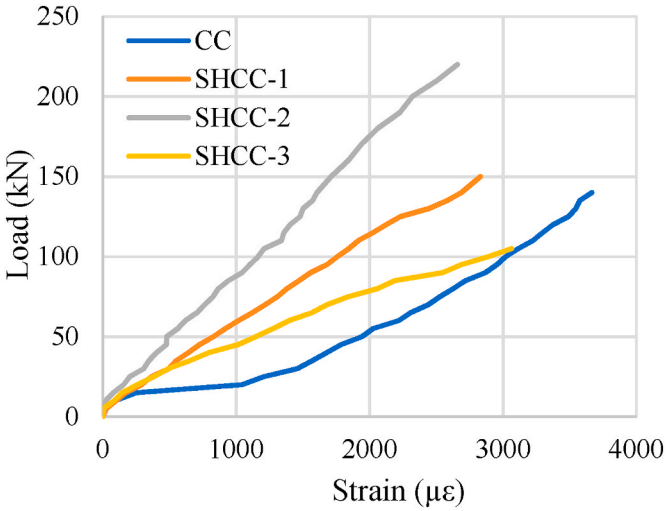

Fig. 12. Load-strain curves of the investigated beam specimens tested under four-point bending.

reduced the strains in the steel bars because the effective cross sectional area of steel bar was increased to resist the same tensile force, thus increasing the load-carrying capacity of the beam.

5. Economic and environmental assessment

This section presents the life-cycle assessment of the material cost and carbon footprint of the adopted SHCC mixture at both the material and the structural levels. Section 5.1 focuses on the life-cycle assessment at the material level. Section 5.2 focuses on the life-cycle assessment at the structural level based on the four tested full-scale beams.

5.1. Materials

This section assesses the unit cost and carbon footprint of the SHCC mixture, and the unit cost and carbon footprint of the conventional concrete mixture used in the fabrication of the tested beams. For comparison, the SHCC mixture and conventional concrete mixture had the same compressive strength. The assessment at the material level considers the cost and carbon footprint of ingredients of the mixtures in the manufacturing and the transportation stages. The cost and carbon footprint of each mixture are respectively calculated as the sum of cost and carbon footprint of the ingredients of the mixture.

The unit cost of each mixture was calculated using Eq. (1):

$$M = \sum_{i=1}^{n} m_i r_i \tag{1}$$

where M is the unit cost of a mixture per cubic meter; m_i is the unit cost of the i-th ingredient ($i = 1, 2, 3, \ldots, n$); and r_i is the mass of the i-th ingredient of the mixture.

The carbon footprint of each mixture was calculated using Eq. (2):

$$C = \sum_{i=1}^{n} c_i r_i \tag{2}$$

where C is the carbon footprint of a mixture per cubic meter; c_i is the unit carbon footprint of the i-th ingredient ($i = 1, 2, 3, \ldots, n$); and r_i is the mass of the i-th ingredient of the mixture.

Table 8 shows the unit cost and carbon footprint of ingredients adopted in the SHCC mixture and conventional concrete mixture. The inventory data were extracted from references (Stengel and Schießl, 2014; Pacheco-Torgal et al., 2014; Van den Heede et al., 2018; Paris et al., 2016).

According to the above inventory data and equations, the unit cost and carbon footprint of the SHCC and conventional concrete mixtures were calculated, as shown in Fig. 13. The cost and carbon footprint of the different SHCC mixtures are compared in Fig. 13(a), indicating that the different mixtures had significantly different costs and carbon footprint. Fig. 13(b) compares the cost and carbon footprint of the optimal SHCC mixture with the conventional concrete with same compressive strength. The results show that the upfront cost and the carbon footprint of the SHCC are higher than that of the conventional concrete. The high upfront cost and carbon footprint are due to the high fiber contents in the SHCC mixtures, and the high cost and carbon footprint are major obstacles of applying the material to engineering structures.

Table 8
Inventory of unit cost and carbon footprint of raw materials.

Ingredient	Cost (USD/kg)	Carbon footprint (kg-CO_2/kg)
Portland cement	0.32	0.83
River sand	0.01	0.001
Coarse aggregate	0.01	0.002
RCP	0.03	0.004
Class F fly ash	0.02	0.001
Quartz sand	0.55	0.03
HRWR	1.82	0.72
Water	0.005	0.001
PVA fiber	12.67	3.40
Basalt fiber	4.31	3.40

5.2. Beams

This section assesses the life-cycle cost and carbon footprint of the beams. The life-cycle assessment of the beams considers the maintenance, repair, and rehabilitation stages of the beams in structural applications, in addition to the manufacturing and transportation of the ingredients. Since the flexural test results showed that the use of SHCC increased the flexural strength of the beams, for the sake of comparison, the material consumption was modified according to the test results of the flexural strength presented in Section 4.3. Specifically, the volumes of the SHCC and steel bars were respectively reduced by 8%. The cost and carbon footprint of the beams in the fabrication stage are elaborated in Section 5.2.1. The cost and carbon footprint of the beams in the maintenance, repair, and rehabilitation stages are elaborated in 5.2.2.

5.2.1. Fabrication stage

The cost and carbon footprint associated with the fabrication of the beams were respectively calculated with the modified volumes. According to the design of beams in Section 4, the volume of a beam was 0.162 m^3, so the volumes of SHCC and conventional concrete were 0.149 m^3 and 0.162 m^3, respectively. With the unit cost and carbon footprint of the mixtures calculated in Section 5.1, the cost and carbon footprint of the SHCC and conventional concrete mixtures were calculated. The cost and carbon footprint of the SHCC were 128 USD and 70 kg, respectively. The cost and carbon footprint of the conventional concrete were 27 USD and 60 kg, respectively.

According to the design of beams in Section 4, the volume of longitudinal steel bars and stirrups in each beam was 1.899×10^{-3} m^3 and 1.125×10^{-3} m^3, so the total volume of steel bars in each beam was 3.024×10^{-3} m^3. The modified volumes of steel bars in the SHCC and conventional concrete beams were 2.782×10^{-3} m^3 and 3.024×10^{-3} m^3, respectively. According to reference (Dong, 2018), the unit cost and carbon footprint of the steel bars were 5.8 USD/kg and 3.03 kg-CO_2/kg. The density of steel is 7800 kg/m^3. The cost and carbon footprint of steel bars of the SHCC beam were calculated to be 126 USD and 66 kg, respectively. The cost and carbon footprint of steel bars of the conventional concrete beam were calculated to be 137 USD and 72 kg, respectively.

The total cost and carbon footprint of the SHCC and the conventional concrete beams were respectively calculated by adding the cost and carbon footprint of SHCC or conventional concrete and the cost and carbon footprint of steel bars in the beams. The cost and carbon footprint of the SHCC beam were 254 USD and 136 kg, respectively. The cost and carbon footprint of the conventional concrete beam were 164 USD and 132 kg, respectively.

5.2.2. Maintenance, repair, and rehabilitation stages

According to engineering practices, the maintenance activities of structures are categorized into preventive maintenance and essential maintenance. Preventive maintenance is performed to slow down deterioration rate. Examples of preventive maintenance include seal joints and cracks. Essential maintenance is performed to deteriorating structures when their performance indicators approach to threshold values. Examples of essential maintenance include repairing or replacement of damaged components. Compared with preventive maintenance, essential maintenance involves more significant efforts and material consumption, and thus essential maintenance has larger effects on structural performance and is accompanied by higher cost. The schedule and scheme of maintenance are associated with the durability of materials and the operation of structures.

When detailed information of durability of materials and operation

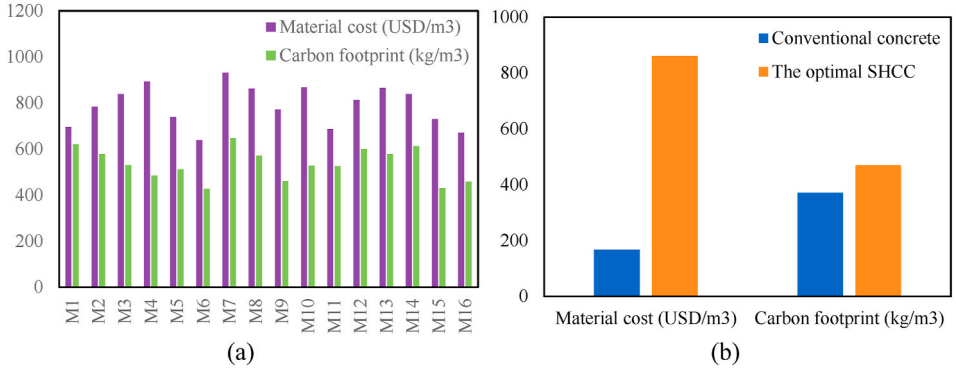

Fig. 13. Results of the life-cycle unit cost and carbon footprint: (a) comparison of the different SHCC mixtures; and (b) comparison of the optimal SHCC mixture with conventional concrete with the same compressive strength.

of structures is available, a precise plan for preventive maintenance and essential maintenance can be made for intended applications. Due to lack of detailed information, the type and frequency of maintenance, repair, and rehabilitation in this study are consistent with normal structures in bridge applications based on historic data, as elaborated in reference (Dong, 2018). The investigated life span of the beam was 75 years. For the beam made using conventional concrete, the intervals of preventive maintenance and essential maintenance were 10 years and 40 years, respectively. The cost and carbon footprint of the preventive maintenance and essential maintenance actions were computed as percentages of the cost and carbon footprint of the fabrication and transportation stages. The percentages were 10% and 50% for the preventive maintenance and essential maintenance actions, respectively. Considering that the SHCC had crack width control and strain-hardening property, the SHCC was anticipated to have higher durability than conventional concrete (Li, 2019). In addition, SHCC mixtures feature self-healing capability, as stated in reference (Li, 2019). Self-healing property further enhances the durability of SHCC. Therefore, the frequencies of the preventive maintenance and the essential maintenance for SHCC beams were considered as a half of the frequencies for conventional concrete beams (Dong, 2018). Over the service life (75 years), the number of preventive maintenance will be three for the SHCC beam and seven for the conventional concrete beam; and the number of essential maintenance will be zero for the SHCC beam and one for the conventional concrete beam.

According to the above analysis, the cost and carbon footprint associated with the maintenance, repair, and rehabilitation stages were respectively calculated to be 76 USD and 41 kg for the reinforced SHCC beam and 197 USD and 158 kg for the conventional reinforced concrete beam. More detailed results are plotted in Fig. 14.

According to Fig. 14(a), as the age of the beam increases, the cost and carbon footprint increase monotonically. The increasing rates of cost and carbon footprint for the conventional reinforced concrete beam are higher than those for the reinforced SHCC beam due to the higher maintenance costs of the conventional reinforced concrete beam. The upfront cost of the reinforced SHCC beam is higher than that of the conventional reinforced concrete beam, but the cost of the reinforced SHCC beam is lower than that of the conventional reinforced concrete beam after the operation time is longer than 40 years. The upfront carbon footprint values of the reinforced SHCC beam and conventional reinforced concrete beam are comparable, but the carbon footprint of the reinforced SHCC beam is lower than that of the conventional reinforced concrete beam after the operation time is longer than 10 years.

6. Conclusions

This research investigates the effects of mixture design variables on the fresh and mechanical properties of SHCC incorporating recycled concrete powder and obtains the optimal mixture. The performance of the SHCC mixture for beam applications is evaluated through flexural tests of beam specimens with different reinforcement ratios. The life-cycle performance of the SHCC mixture and beams with recycled concrete powder is investigated in terms of life-cycle unit cost, carbon footprint, and energy consumption. Based on the above investigations, the following conclusions are drawn:

- For the investigated mixtures, the RCP content showed the highest effects on the fresh and mechanical properties of SHCC mixtures, followed by water-to-binder ratio and fiber content. When RCP with particle size finer than cement was used to prepare SHCC, increasing the RCP content reduced the flowability and mechanical strengths of SHCC matrix but increased the ductility. Such results were different from previous research that indicated opposite changing trends of the mechanical strengths and ductility when RCP was used in preparing SHCC. Although RCP was capable of promoting hydration

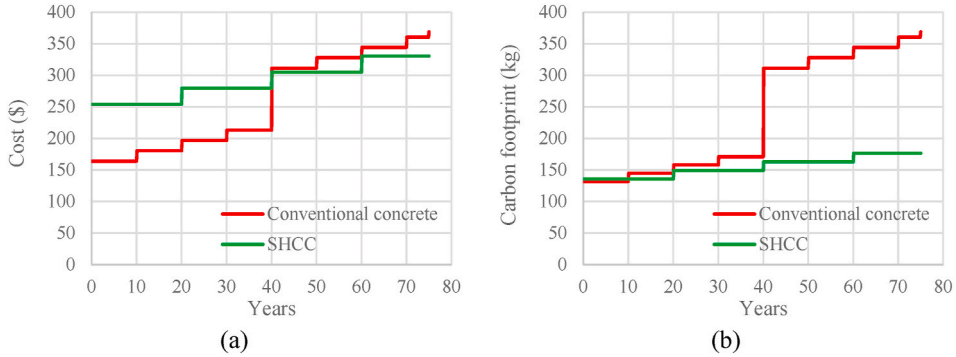

Fig. 14. Life-cycle assessment results of the SHCC beam and conventional concrete beam: (a) life-cycle cost, and (b) carbon footprint.

reactions, the low flowability entrapped air and generated defects in the matrix.

- The beam made with SHCC exhibited higher load-carrying capacity and crack resistance than the beam made with conventional concrete and the same reinforcement ratio. When the reinforcement ratio was 1%, the load-carrying capacity was increased by 8% by using the SHCC. The enhancement is attributed to the tension resistance of the SHCC after it is cracked, and the tension resistance alleviated the tensile force applied to the longitudinal steel bars near the cracked sections. Increasing the reinforcement ratio in SHCC beams was effective in further enhancing the load-carrying capacity and improving crack pattern.
- According to the life-cycle assessment, the SHCC incorporating RCP had higher upfront cost and lower carbon footprint than the conventional concrete with the same compressive strength. The upfront cost of the reinforced SHCC beam is higher than that of conventional reinforced concrete beam, but the cost of the reinforced SHCC beam is lower than that of the conventional reinforced concrete beam after the operation time is longer than 40 years. The carbon footprint of the SHCC beam is higher than that of the conventional concrete beam throughout the lifetime.

CRediT authorship contribution statement

Xiuling Li: Conceptualization, Data curation, Formal analysis, Funding acquisition, Investigation, Resources, Software, Validation, Visualization, Writing – original draft. **Xiangrong Lv:** Data curation, Investigation, Software, Writing – review & editing. **Xintao Zhou:** Validation, Writing – review & editing. **Weina Meng:** Conceptualization, Funding acquisition, Resources, Writing – review & editing. **Yi Bao:** Conceptualization, Methodology, Project administration, Supervision, Writing – review & editing.

Declaration of competing interest

The authors declare that they have no known competing financial interests or personal relationships that could have appeared to influence the work reported in this paper.

Acknowledgement

This research was funded by Natural Science Foundation of China [grant number 51278290], Natural Science Foundation of Shandong Province [grant number ZR2020ME245], Institute of Engineering Mechanics of the China Earthquake Administration [grant number 2019D10], and National Science Foundation [grant number CMMI-2046407].

Appendix

The tensile stress-strain curves of the 16 mixtures tested in direct tensile tests at 28 days are presented in this appendix. The test method is elaborated in Section 3.3. Table 4 lists the results of the tensile strength and ductility extracted from the stress-strain curves.

References

Adams, M.P., Jones, A., Beauchemin, S., Johnson, R., Fournier, B., Shehata, M., et al., 2013. Applicability of the accelerated mortar bar test for alkali-silica reactivity of recycled concrete aggregates. Advances in Civil Engineering Materials 2 (1), 78–96.

Adesina, A., Das, S., 2021. Evaluation of the durability properties of engineered cementitious composites incorporating recycled concrete as aggregate. J. Mater. Civ. Eng. 33 (2), 04020439.

Assi, L.N., Deaver, E.E., Ziehl, P., 2018. Effect of source and particle size distribution on the mechanical and microstructural properties of fly Ash-Based geopolymer concrete. Construct. Build. Mater. 167, 372–380.

Bao, Y., Chen, G., 2015. Strain distribution and crack detection in thin unbonded concrete pavement overlays with fully distributed fiber optic sensors. Opt. Eng. 55 (1), 011008.

Bao, Y., Li, V.C., 2020. Feasibility study of Lego-inspired construction with bendable concrete. Autom. ConStruct. 113, 103161.

Dong, Y., 2018. Performance assessment and design of ultra-high performance concrete (UHPC) structures incorporating life-cycle cost and environmental impacts. Construct. Build. Mater. 167, 414–425.

Etxeberria, M., Marí, A.R., Vázquez, E., 2007. Recycled aggregate concrete as structural material. Mater. Struct. 40 (5), 529–541.

Gao, D., Lv, M., Yang, L., Tang, J., Chen, G., Meng, Y., 2020. Experimental study of utilizing recycled fine aggregate for the preparation of high ductility cementitious composites. Materials 13 (3), 679.

Gao, D., Lv, M., Yang, L., Tang, J., 2021. Flexural properties of high ductility cementitious composites with totally recycled fine aggregate. J. Mater .Res.Technol 14, 1319–1332. https://doi.org/10.1016/j.jmrt.2021.07.047.

Gencel, O., Erdugmus, E., Sutcu, M., Oren, O.H., 2020. Effects of concrete waste on characteristics of structural fired clay bricks. Construct. Build. Mater. 255, 119362.

Guo, P., Bao, Y., Meng, W., 2021. Review of using glass in high-performance fiber-reinforced cementitious composites. Cement Concr. Compos. 104032.

GB/T 1596-2017, 2017. Fly Ash Used for Cement and Concrete.

GB/T 176-2017, 2017. Methods for Chemical Analysis of Cement.

GB/T 208-2014, 2014. Test Method for Determining Cement Density.

GB/T 2419-2005, 2005. Test Method for Fluidity of Cement Mortar. Beijing, China.

He, Z., Shen, A., Wu, H., Wang, W., Wang, L., Yao, C., et al., 2021. Research progress on recycled clay brick waste as an alternative to cement for sustainable construction materials. Construct. Build. Mater. 274, 122113.

Ho, H.J., Iizuka, A., Shibata, E., 2020. Chemical recycling and use of various types of concrete waste: a review. J. Clean. Prod. 124785.

JGJ/T70-2009, 2009. Standard for Test Method of Performance on Building Mortar.

Ji, J., Song, H., Jiang, L., Ren, H., Zhang, Y., Liu, Y., 2021. Tensile performance of high ductility cementitious composites with recycled powder from C&D waste. Frontiers in Materials 8, 98.

Keppert, M., Davidová, V., Doušová, B., Scheinherrová, L., Reiterman, P., 2021. Recycling of fresh concrete slurry waste as supplementary cementing material: characterization, application and leaching of selected elements. Construct. Build. Mater. 300, 124061.

Khayat, K.H., Meng, W., Vallurupalli, K., Teng, L., 2019. Rheological properties of ultra-high-performance concrete—an overview. Cement Concr. Res. 124, 105828.

Korf, N., Løvik, A.N., Figi, R., Schreiner, C., Kuntz, C., Mählitz, P.M., et al., 2019. Multi-element chemical analysis of printed circuit boards–challenges and pitfalls. Waste Manag. 92, 124–136.

Le, H.B., Bui, Q.B., 2020. Recycled aggregate concretes–a state-of-the-art from the microstructure to the structural performance. Construct. Build. Mater. 257, 119522.

Li, V.C., 2003. On engineered cementitious composites (ECC) a review of the material and its applications. J. Adv. Concr. Technol. 1 (3), 215–230.

Li, V.C., 2019. Engineered Cementitious Composites (ECC): Bendable Concrete for Sustainable and Resilient Infrastructure. Springer.

Li, J., Yang, E.H., 2017. Macroscopic and microstructural properties of engineered cementitious composites incorporating recycled concrete fines. Cement Concr. Compos. 78, 33–42.

Li, X., Wang, J., Bao, Y., Chen, G., 2017a. Cyclic behavior of damaged reinforced concrete columns repaired with high-performance fiber-reinforced cementitious composite. Eng. Struct. 136, 26–35.

Li, X., Bao, Y., Xue, N., Chen, G., 2017b. Bond strength of steel bars embedded in high-performance fiber-reinforced cementitious composite before and after exposure to elevated temperatures. Fire Saf. J. 92, 98–106.

Li, X., Bao, Y., Wu, L., Yan, Q., Ma, H., Chen, G., et al., 2017c. Thermal and mechanical properties of high-performance fiber-reinforced cementitious composites after exposure to high temperatures. Construct. Build. Mater. 157, 829–838.

Li, X., Xu, H., Meng, W., Bao, Y., 2018. Tri-axial compressive properties of high-performance fiber-reinforced cementitious composites after exposure to high temperatures. Construct. Build. Mater. 190, 939–947.

Li, X., Xu, Z., Bao, Y., Cong, Z., 2019. Post-fire seismic behavior of two-bay two-story frames with high-performance fiber-reinforced cementitious composite joints. Eng. Struct. 183, 150–159.

Li, X., Li, Y., Yan, M., Meng, W., Lu, X., Chen, K., Bao, Y., 2021. Cyclic Behavior of Joints Assembled Using Prefabricated Beams and Columns with Engineered Cementitious Composite (ECC). Engineering Structures, p. 113115.

Limbachiya, M.C., Leelawat, T., Dhir, R.K., 2000. Use of recycled concrete aggregate in high-strength concrete. Mater. Struct. 33 (9), 574–580.

Liu, Z., Meng, W., 2021. Fundamental understanding of carbonation curing and durability of carbonation-cured cement-based composites: a review. J .CO2. Utilization 44, 101428.

Liu, J.C., Tan, K.H., 2018. Mechanism of PVA fibers in mitigating explosive spalling of engineered cementitious composite at elevated temperature. Cement Concr. Compos. 93, 235–245.

Ma, Z., Liu, M., Duan, Z., Liang, C., Wu, H., 2020. Effects of active waste powder obtained from C&D waste on the microproperties and water permeability of concrete. J. Clean. Prod. 257, 120518.

Meng, W., Khayat, K., 2017. Effects of saturated lightweight sand content on key characteristics of ultra-high-performance concrete. Cement Concr. Res. 101, 46–54.

Meng, W., Valipour, M., Khayat, K.H., 2017. Optimization and performance of cost-effective ultra-high performance concrete. Mater. Struct. 50 (1), 1–16.

Pacheco-Torgal, F., Cabeza, L.F., Labrincha, J., De Magalhaes, A.G., 2014. Eco-efficient Construction and Building Materials: Life Cycle Assessment (LCA), Eco-Labelling and Case Studies. Woodhead Publishing.

Paris, J.M., Roessler, J.G., Ferraro, C.C., DeFord, H.D., Townsend, T.G., 2016. A review of waste products utilized as supplements to Portland cement in concrete. J. Clean. Prod. 121, 1–18.

Sagoe-Crentsil, K.K., Brown, T., Taylor, A.H., 2001. Performance of concrete made with commercially produced coarse recycled concrete aggregate. Cement Concr. Res. 31 (5), 707–712.

Stengel, T., Schießl, P., 2014. Life cycle assessment (LCA) of ultra high performance concrete (UHPC) structures. In: Eco-efficient Construction and Building Materials. Woodhead Publishing, pp. 528–564.

Tabsh, S.W., Abdelfatah, A.S., 2009. Influence of recycled concrete aggregates on strength properties of concrete. Construct. Build. Mater. 23 (2), 1163–1167.

Tan, X., Abu-Obeidah, A., Bao, Y., Nassif, H., Nasreddine, W., 2021. Measurement and visualization of strains and cracks in CFRP post-tensioned fiber reinforced concrete beams using distributed fiber optic sensors. Autom. ConStruct. 124, 103604.

Thomas, C., Setién, J., Polanco, J., Alaejos, P., De Juan, M.S., 2013. Durability of recycled aggregate concrete. Construct. Build. Mater. 40, 1054–1065.

Trottier, C., Zahedi, A., Ziapour, R., Sanchez, L., Locati, F., 2021. Microscopic assessment of recycled concrete aggregate (RCA) mixtures affected by alkali-silica reaction (ASR). Construct. Build. Mater. 269, 121250.

U.S. EPA. Construction and Demolition Debris: Material-specific Data. https://www.epa.gov/sites/default/files/2021-01/documents/2018_ff_fact_sheet_dec_2020_fnl_508.pdf.

Van den Heede, P., Mignon, A., Habert, G., De Belie, N., 2018. Cradle-to-gate life cycle assessment of self-healing engineered cementitious composite with in-house developed (semi-) synthetic superabsorbent polymers. Cement Concr. Compos. 94, 166–180.

Wang, Y., Zhang, Z., Yu, J., Xiao, J., Xu, Q., 2019. Using green supplementary materials to achieve more ductile ECC. Materials 12 (6), 858.

Wong, C.L., Mo, K.H., Yap, S.P., Alengaram, U.J., Ling, T.C., 2018. Potential use of brick waste as alternate concrete-making materials: a review. J. Clean. Prod. 195, 226–239.

Wu, R., Zhao, T., Zhang, P., Yang, D., Liu, M., Ma, Z., 2021. Tensile behavior of strain hardening cementitious composites (SHCC) containing reactive recycled powder from various C&D waste. J.Renewable .Mater 9 (4), 743.

Xu, M., Bao, Y., Wu, K., Xia, T., Clack, H.L., Shi, H., Li, V.C., 2019a. Influence of TiO2 incorporation methods on NOx abatement in engineered cementitious composites. Construct. Build. Mater. 221, 375–383.

Xu, M., Bao, Y., Wu, K., Shi, H., Guo, X., Li, V.C., 2019b. Multiscale investigation of tensile properties of a TiO2-doped engineered cementitious composite. Construct. Build. Mater. 209, 485–491.

Xu, M., Clack, H., Xia, T., Bao, Y., Wu, K., Shi, H., Li, V., 2020. Effect of TiO2 and fly ash on photocatalytic NOx abatement of engineered cementitious composites. Construct. Build. Mater. 236, 117559.

Yu, L., Huang, L., Ding, H., 2019a. Rheological and mechanical properties of ultra-high-performance concrete containing fine recycled concrete aggregates. Materials 12 (22), 3717. [14].

Yu, K., Zhu, W., Ding, Y., Lu, Z., Yu, J., Xiao, J., 2019b. Micro-structural and mechanical properties of ultra-high performance engineered cementitious composites (UHP-ECC) incorporation of recycled fine powder (RFP). Cement Concr. Res. 124, 105813.

Yu, J., Jiang, F., Yu, K., Dong, F., Duan, X., 2020. Deformability enhancement of fiber-reinforced cementitious composite by incorporating recycled powder. J. Reinforc. Plast. Compos. 39 (3–4), 119–131.

Zhang, Z., Qian, S., Ma, H., 2014. Investigating mechanical properties and self-healing behavior of micro-cracked ECC with different volume of fly ash. Construct. Build. Mater. 52, 17–23.